

# Effect of uniform distributions of bonded and debonded fibers on the growth of the fiber/matrix interface crack in thin UD laminates with different fiber contents under transverse loading

Luca Di Stasio<sup>a,b</sup>, Janis Varna<sup>b</sup>, Zoubir Ayadi<sup>a</sup>

<sup>a</sup>Université de Lorraine, EEIGM, IJL, 6 Rue Bastien Lepage, F-54010 Nancy, France

<sup>b</sup>Luleå University of Technology, University Campus, SE-97187 Luleå, Sweden

---

## Abstract

*Priority: 1*

*Target journal(s):* Composites Part B: Engineering, Composites Part A: Applied Science and Manufacturing, Composite Structures, Journal of Composite Materials, Composite Communications

---

## 1. Introduction

1. We start with a few lines devoted to the spread tow technology and thin plies: what they are, what can be done, what are the possible applications.
- 5 2. By quoting the relevant references, we report on the observation that one of the main beneficial mechanisms in thin ply is the retardation of transverse crack propagation. We then enlarge by reporting the microscopical observations by Saito, in which debonds where also observed. We observe that available microscopic observations are just a few and mainly in 2D.
- 10 3. Propagation of transverse cracks has been widely investigated both analytically and numerically
4. Initiation at the level of fiber/matrix interface is instead a less researched subject.

5. cohesive elements are a possible choice, but have some drawbacks, which  
15 makes a LEFM approach valuable
6. With regard to LEFM studies of laminates under transverse loading, models can be found in the literature about: the single fiber in infinite matrix under different mode of loading, the effect of adjacent fibers on a fiber in infinite matrix under different mode of loading, the single fiber in an  
20 equivalent composite in transverse tension, the effect of adjacent fibers on a fiber in an equivalent composite in transverse tension.
7. For initiation of transverse cracking at the fiber/matrix interface in UD laminates under transverse tension, there is thus a gap regarding: the effect of fiber volume fraction; the interaction of debonded and bonded  
25 fibers in micro-structured assemblies, i.e. no homogenization. This article addresses these two points.
8. We conclude the introduction with a summary of the article's structure.

## 2. RVE models & FE discretization

### 2.1. Introduction & Nomenclature

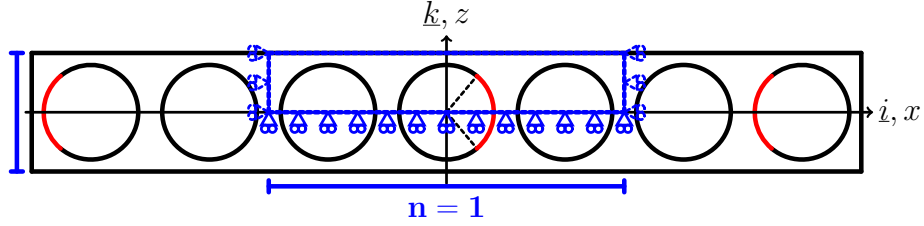
30 In this paper, we analyze debond development in unidirectional (UD) composites subjected to in-plane transverse tensile loading. The interaction between debonds in UD composites is studied developing models of different Repeating Unit Cells (RUC) of laminates where only the central fiber in the cell has a damage in the form of a fiber/matrix interface crack (debond). The composite RUC may be repeating in the transverse direction only (representing an  
35 ultra-thin composite) or repeating also in the composite thickness direction, representing an infinite composite in a limiting case. Thus, the conditions at the UD composite's upper and lower boundaries are one of the parameters for the investigation. The used RUCs allow for the consideration of the composite  
40 with debonds as a sequence of damaged and undamaged rows, each row with only one fiber in the thickness direction. Since all of these RUCs feature regular microstructures with fibers placed according to a square-packing tiling, they

are Representative Volume Elements (RVE) of composites with a certain distribution of debonds. Introducing in-plane coordinates  $x$  and  $y$ , where  $x$  is in the transverse direction of the UD composite under consideration, the strain in the  $y$ -direction due to a load in the  $x$ -direction is small, due to the very small minor Poissons ratio of the UD composite. Additionally, debonds are considered to be significantly longer in the fiber direction than in the arc direction. Therefore, we use 2D models under the assumption of plane strain, defined in the  $x - z$  section of the composite. Thus, the analysis presented applies to long debonds, with a focus on understanding the mechanisms of growth along its arc direction. The composites are subjected to transverse tensile strain, applied as a constant displacement in the  $x$ -direction along the vertical boundary of the RUC as shown in Figure 1 to 4. As the models are differentiated by the number of layers of fibers and by the spacing between debonds along the vertical and horizontal directions, the corresponding RUCs can be distinguished from each other based on the number  $n$  of fibers in the horizontal direction and  $k$  in the vertical direction. Furthermore, the horizontal surfaces can be either free or vertical displacement coupling can be applied. We thus introduce the common notation  $n \times k - free$  and  $n \times k - coupling$  to denote a RUC with  $n \times k$  fibers and, respectively, a free upper surface or kinematic coupling applied to it. The specific combinations of particular choices of  $n$ ,  $k$ , and boundary conditions are detailed in Section 2.2, together with the corresponding models of damaged composite they are representing.

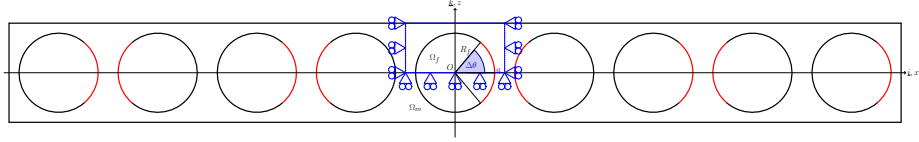
## 2.2. Models of Representative Volume Element (RVE)

The first two models feature, as shown in Fig. 1, an ultra-thin UD laminate with only one row of fibers across its thickness,  $k = 1$ . This is quite an extreme model from the microstructural point of view; however, it allows to focus the analysis on the interaction between debonded fibers placed along the  $x$ -direction. Furthermore, as the horizontal surfaces are considered free, the interaction is stronger in this case than in any other, making the predictions of this model rather conservative. In retrospective, if only 20 years ago such a model would

have been considered too abstracted from the physical reality, the recent advancements in the spread tow technology make this approach appealing also as  
75 a limiting case for practical considerations.



(a) Single row of fibers with a debond appearing every  $m$  fibers.

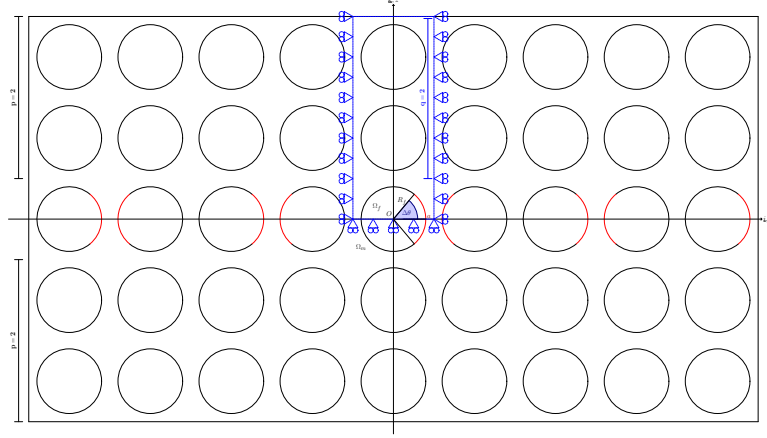


(b) Single row of fibers with debonds appearing on each fiber.

Figure 1: Models of ultra-thin UD composites with a single “row” of fibers and debonds repeating at different distances. The corresponding repeating element (RUC) is highlighted in blue, while debonds are represented in red.

In the first sub-model, Fig. 1a, every  $n^{th}$  fiber in the composite is partially debonded on alternating sides of the fiber. The symmetries of the model allow the use of the upper part of the RUC. It is highlighted by blue lines in Fig. 1 to 3. Following the notation introduced in Section 2.1, we will refer to this  
80 model as  $n \times 1 - free$ . In the second sub-model  $n = 1$ , Fig. 1b, and a debond appears on each fiber on alternating sides and the corresponding RUC contains only one fiber. We will refer to this model as  $1 \times 1 - free$ .

The second set of models in Fig. 2 and Fig. 3 considers laminates with multiple rows of fibers across the thickness: a finite number of rows in the first  
85 two sub-models in Fig. 2; an infinite number in the model of Fig. 3. In Fig. 2a, the RUC contains  $n = 1$  fiber in the x-direction,  $k$  fibers across the thickness and the central fiber is debonded. This model will be referred to in the following as  $1 \times k - free$ . Thinking in terms of rows, in this model we have a central



(a) Multiple rows of fibers with debonds appearing on each fiber belonging to the central row.



(b) Mutiple rows of fibers with a debond appearing every  $m$  fibers within the central row.

Figure 2: Models of UD composites with different “rows” of fibers and debonds repeating at different distances. The corresponding repeating element (RUC) is highlighted in blue, while debonds are represented in red.

row where each fiber is debonded. This row is surrounded from each side by  
90  $(k-1)/2$  rows with perfectly bonded fibers. In the sub-model in Fig. 2b, each  $n^{th}$   
fiber in the central row is debonded and this row is surrounded by  $(k-1)/2$  rows  
of undamaged fibers from each side. We will refer to this model as  $n \times k - free$   
(because the horizontal boundary of the RUC is free of any constraint).

Finally, the model in Fig. 3 considers an UD composite with an infinite



Figure 3: Model of UD composites with an infinite number of “rows” of fibers and debonds appearing on each fiber. The corresponding repeating element (RUC) is highlighted in blue, while debonds are represented in red.

95 number of rows; all of them with partially debonded fibers. As all fibers have debonds, the corresponding RUC is made of a single partially debonded fiber with kinematic coupling conditions applied to the upper boundary to assure periodicity. This model is referred to as  $1 \times 1$  – *coupling*.

### 2.3. Finite Element (FE) discretization

100 Each RUC is discretized using the Finite Element Method (FEM) within the Abaqus environment, a commercial FEM package [1]. The length  $l$  and height  $h$  of the model are determined by number of fibers  $n$  in the horizontal direction and  $k$  across the thickness (see 2.2) according to Eq. 1:

$$l = 2nL \quad h = 2kL; \quad (1)$$

where the reference length  $L$ , see Fig. 4a, is defined as a function of the fiber 105 volume fraction  $V_f$  and the fibers’ radius according to

$$L = \frac{R_f}{2} \sqrt{\frac{\pi}{V_f}}. \quad (2)$$

The fibers’ radius  $R_f$  is assumed to be the same for each fiber present in the model and equal to  $1 \mu m$ . The latter value is not physical and it has been chosen for simplicity. It is worth to note at this point that, in a linear elastic

solution as the one presented here, the ERR is proportional to the geometrical  
 110 dimensions and recalculation of the ERR for fibers of any size thus requires  
 a simple multiplication. Furthermore, notice that the relationships in Eqs. 1  
 and 2 ensure that the local and global  $V_f$  are everywhere equal.

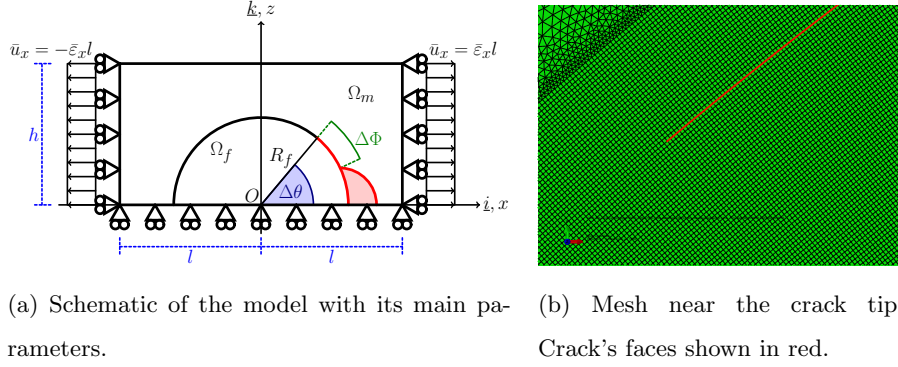


Figure 4: Details and main parameters of the Finite Element model.

The debond is placed symmetrically with respect to the  $x$  axis (in red in 4a) and has an angular size of  $\Delta\theta$  (the full debond's size is thus  $2\Delta\theta$ ). For large  
 115 debond's sizes ( $\geq 60^\circ - 80^\circ$ ), a region of variable size  $\Delta\Phi$  appears at the crack  
 tip in which the crack's faces are in contact and slide on each other. Due to  
 its appearance, frictionless contact is considered between the two crack's faces  
 to allow free sliding and avoid interpenetration. Symmetry with respect to  
 the  $x$  axis is applied on the lower boundary and kinematic coupling on the  $x$ -  
 120 displacement along the left and right sides. The upper boundary is in general  
 free, except for the model  $1 \times 1 - coupling$  (Fig. 3) which requires kinematic  
 coupling of vertical displacements also on the upper side. Constant transverse  
 strain  $\bar{\epsilon}$  equal to 1% is applied to the right and left sides by means of an imposed  
 $x$ -displacement of, respectively,  $\pm\bar{\epsilon}l$ .

125 The model is meshed using second order, 2D, plane strain triangular (CPE6)  
 and rectangular (CPE8) elements. A regular mesh of quadrilateral elements  
 with an almost unitary aspect ratio is required at the crack tip, as shown in  
 Fig. 4b. The angular size  $\delta$  of an element in the crack tip region is always

Table 1: Summary of the mechanical properties of fiber and matrix.

<b>Material</b>	$E$ [GPa]	$G$ [GPa]	$\nu$ [-]
Glass fiber	70.0	29.2	0.2
Epoxy	3.5	1.25	0.4

equal to  $0.05^\circ$ . The Mode I, Mode II and total Energy Release Rates (ERRs) (respectively referred to as  $G_I$ ,  $G_{II}$  and  $G_{TOT}$ ) represent the main output of the FEM analysis; they are evaluated using the VCCT technique [2] implemented in a custom Python routine and, for the total ERR, the J-integral [3] by application of the Abaqus built-in functionality. A glass fiber-epoxy system is considered in every model, and it is assumed that their response lies always in the linear elastic domain. The properties used are listed in Table 1.

#### 2.4. Validation of the model

The model is validated in Fig. 5 against the results reported in [4], obtained with the Boundary Element Method (BEM) for a single fiber with a symmetric debond placed in an infinite matrix. This situation is modeled using the *free* RVE with  $V_f = 0.0079\%$ , which corresponds to a RUC's length and height of  $\sim 100$ .

To allow for a comparison, the results are normalized following [4] with respect to a reference Energy Release Rate  $G_0$  defined as

$$G_0 = \frac{1 + k_m}{8\mu_m} \sigma_0^2 \pi R_f \quad (3)$$

where  $\mu$  is the shear modulus,  $k$  is the Kolosov's constant defined as  $3 - 4\nu$  for plane strain conditions,  $R_f$  is the fiber radius and the index  $m$  refers to the properties of the matrix.  $\sigma_0$  is the stress at the boundary, computed as the average of the stress extracted at each boundary node along the right side (arithmetic average as nodes are equispaced by design along both the left and right sides). The agreement is good: the difference between the BEM solution, which is considered more accurate, and the FEM solution does not exceed 5%.



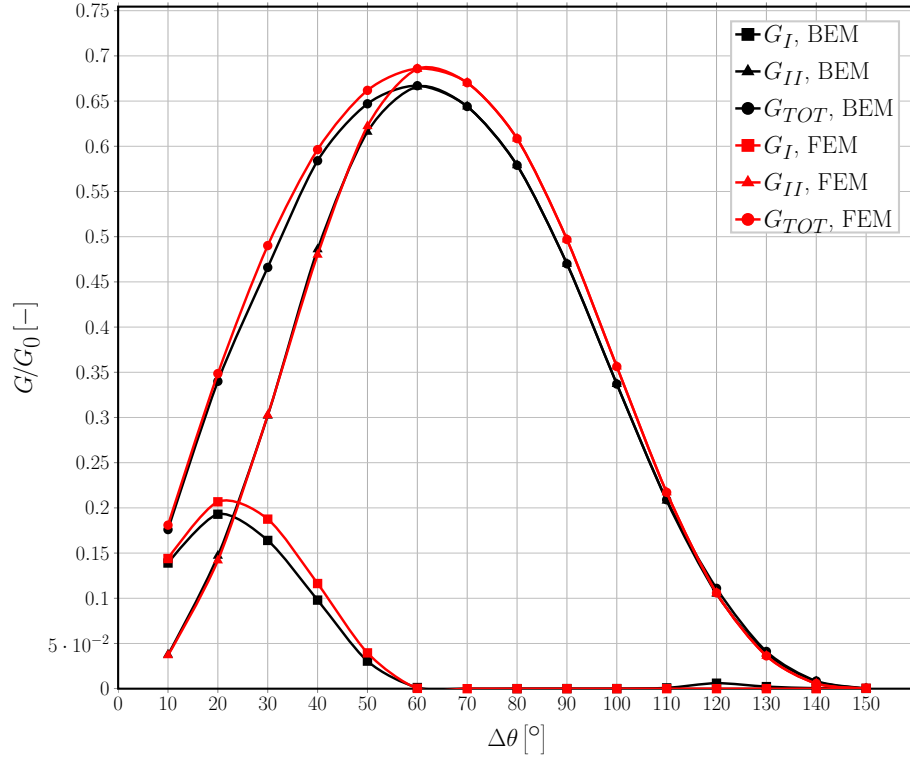


Figure 5: Validation of the single fiber model for the infinite matrix case with respect to the BEM solution in [4].

The ERRs' maxima are in the same positions and the size of the contact zone is the same. Nevertheless, an analysis of phenomena leading to less than 5% differences in ERR would not be reliable and, therefore, it is not recommended.

### 3. Results & Discussion

#### 3.1. Effect of Fiber Volume Fraction

As shown in Figs. 6 and 7, respectively for Mode I and Mode II, the fiber content has a drastic effect on the Energy Release Rate at the tip of the fibre/matrix interface crack. The effect of four levels of fiber volume fraction are compared, 30%, 50%, 60% and 65%, on two microstructural models: a  $11 \times 11$  – *free* (every 11<sup>th</sup> fiber in the central fiber row is partially debonded and, on the top of this

row, we have 5 undamaged fiber rows), Figs. 6a and 7a, and a  $21 \times 21 - free$  (every  $21^{th}$  fiber in the central fiber row is partially debonded and, on the top of this row, we have 10 undamaged fiber rows), Figs. 6b and 7b.

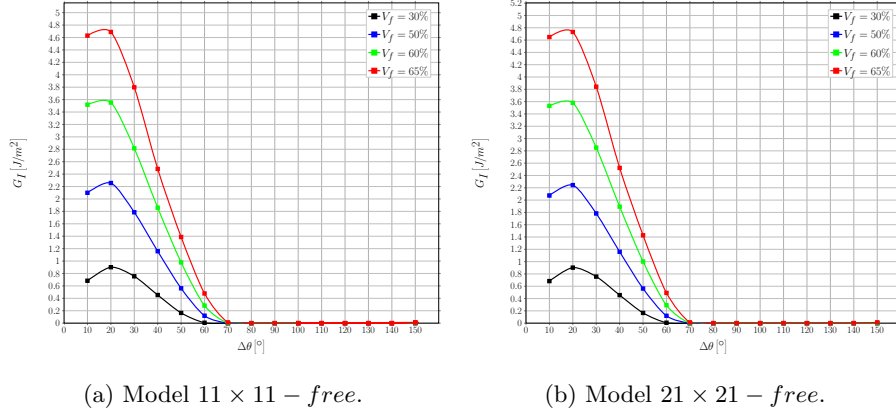


Figure 6: A view of the effect of fiber volume fraction on Mode I ERR in two exemplificative models, subject to an applied transverse strain  $\varepsilon_x$  of 1%.

Comparing Fig. 6a with 6b, and Fig. 7a with 7b, we can observe that the ERRs' values are very similar for RUCs with  $11 \times 11$  and  $21 \times 21$  fibers, though they are slightly higher for the larger RUC where the next debonded fiber and the free surface are further away from the debonded fiber. From these results we conclude that both RUCs are large enough to represent a single debonded fiber in an infinite array of bonded fibers. Obviously, there exists a specific effect of the fiber content. For Mode I, Fig. 6, the maximum value of the ERR increases by  $\sim 5.2$  times when  $V_f$  changes from 30% to 65%. The debond's angular size for which the peak value occurs remains unchanged at  $20^\circ$ , but for  $V_f = 60\%$  and  $65\%$  the Mode I ERR at  $10^\circ$  and at  $20^\circ$  are rather similar, approximately creating a plateau. Furthermore, increasing the fiber volume fraction delays the onset of the contact zone, which corresponds in Fig. 6 to the first value of  $\Delta\theta$  for which  $G_I$  is equal to zero. For  $V_f = 30\%$ , the contact zone first appears for a debond of  $60^\circ$ , similarly to what happens in the single fiber in infinite matrix model (Fig. 5). For higher fiber contents, the contact zone's onset is delayed to

a debond's size approximately equal to  $70^\circ$ .

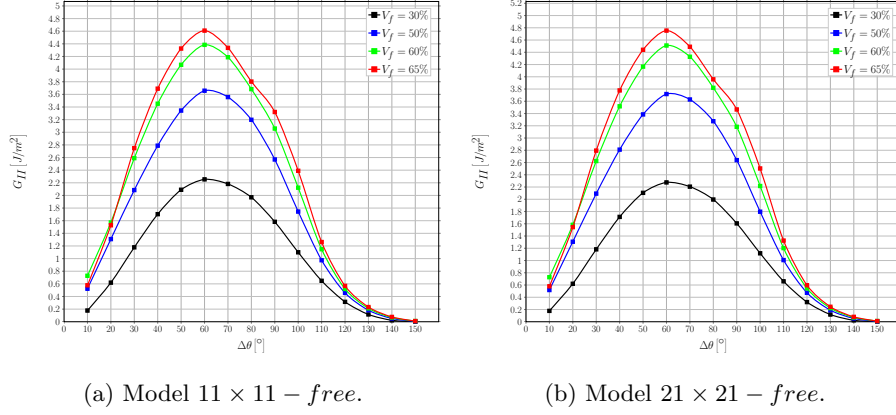


Figure 7: A view of the effect of fiber volume fraction on Mode II ERR in two exemplificative models, subject to an applied transverse strain  $\varepsilon_x$  of 1%.

For Mode II, Fig. 7, the maximum value of the ERR is increases by  $\sim 2.1$  times when  $V_f$  changes from 30% to 65%. The effect is thus similar to Mode I, but with a significantly lower magnitude. Similar to Mode I, the debond's size for which the peak value of Mode II occurs remains unchanged, at  $60^\circ$  for Mode II. There is a distinct maximum in the curve and its shape does not dependon the fiber content. It is worthwhile to notice that the ratio of Mode II to Mode I peak values is  $\frac{\max(G_{II})}{\max(G_I)} \sim \frac{2.2}{0.9} \sim 2.4$  for  $V_f = 30\%$ , while it is  $\sim \frac{4.7}{4.7} \sim 1$  for  $V_f = 65\%$ . Given that the peaks occur at different debond's sizes, for which the value of the other ERR is very small or even close to zero, this means that the increase in fiber content creates a long range of very close values of the total ERR, that may have a global destabilizing effect on the debond's growth.

The general increasing trends observed in Figs. 6 and 7 are related to the fact that, given that the global and local  $V_f$  are everywhere identical in the models presented, an increase in fiber content corresponds to a decrease in the average distance between fibers. Thus, the decay of the local stress and strain fields in the matrix domain occurs over smaller lengths causing higher values at the crack tip. The difference in relative magnification between Mode I and Mode II and the delay in the contact zone's onset are instead due to the interplay

between two different mechanisms, both caused by the ordered microstructural arrangement of the model. In the models considered, a fully bonded fiber is always placed along the horizontal direction, aligned with the partially debonded fiber and exactly in front of the debond. By increasing  $V_f$ , the former moves closer to the latter and for small debonds this causes a magnification of the  $x$ -strain at the crack tip. For small debonds ( $\leq 20^\circ - 30^\circ$ ) in fact, the crack tip is approximately normal to the  $x$ -direction and thus an increase in  $\varepsilon_x$  causes an increase in  $G_I$ . On the other hand, for large debonds ( $\geq 70^\circ - 80^\circ$ ) the crack growth direction is almost aligned with the  $x$ -axis, thus a magnification in the  $x$ -strain translates into an increase of Mode II ERR. However, this increasing effect on  $G_{II}$  is partially counteracted by the presence of a fully bonded fiber on top of the debonded fiber and aligned with it. As fibers are more rigid than the surrounding matrix, the presence of the former will restrain horizontal displacements, thus hampering strong increases in  $G_{II}$  for large debonds. Furthermore, due to the mismatch in the Poisson's ratios, the fully bonded fiber placed above generates an upward-directed component of the vertical displacement field in the matrix, which tends to open the debond and causes the delay in the contact zone's onset. The interplay between these mechanisms is governed by the average inter-fiber distance and, in turn, by the fiber volume fraction.

### 3.2. Interaction between debonds in UD laminates with a single layer of fibers

The interaction of debonds appearing at regular intervals in an ultra-thin UD composite with a single row of fibers is studied for Mode I (Fig. 8) and Mode II (Fig. 9) and fiber content equal to 30% (Figs. 8a and 9a) and 60% (Figs. 8b and 9b). The models treated are  $3 \times 1 - free$ ,  $5 \times 1 - free$ ,  $7 \times 1 - free$ ,  $11 \times 1 - free$ ,  $21 \times 1 - free$ ,  $101 \times 1 - free$  and  $201 \times 1 - free$ , corresponding respectively to a debond every  $3^{rd}$ ,  $5^{th}$ ,  $7^{th}$ ,  $11^{th}$ ,  $21^{st}$ ,  $101^{st}$  and  $201^{st}$  fiber (Fig. 1a). Given that the upper surface of the UD row is left free, the interaction with the next RUC is stronger than in any other case and the results of this section are thus the most conservative in terms of debond's growth: the ERRs should be the largest. The effect is enhanced in composites with high  $V_f$  and

especially for  $G_{II}$ : at  $V_f = 60\%$  the highest  $G_{II}$  value for the  $201 \times 1 - free$  composite in Fig. 9b is more than 3 times higher than the  $G_{II}$  value for the  $21 \times 21 - free$  composite in Fig. 7b. Even the maximum is shifted to larger angles. The  $G_I$  value is only 30% higher.

From both Fig. 8 and Fig. 9, it can be seen that the presence of a debond decreases the strain magnification effect discussed in Sec. 3.1 and thus reduces the value of the ERR. This phenomenon is called “crack shielding”.

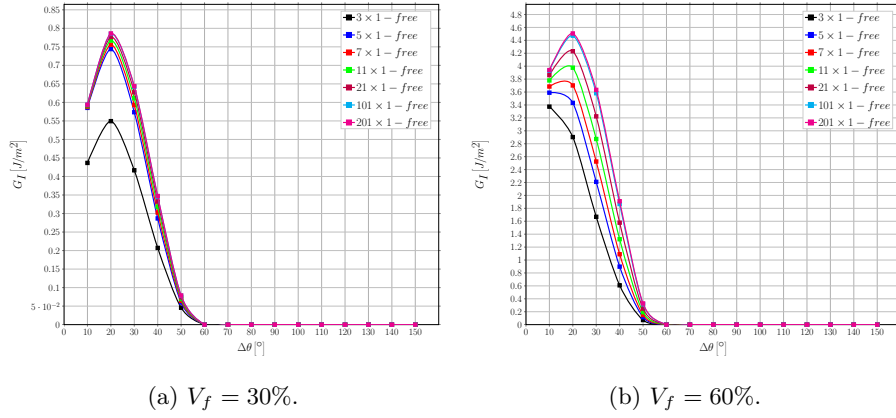


Figure 8: Effect of the interaction between debonds appearing at regular intervals on Mode I ERR in an UD with a single layer of fibers at different levels of fiber volume fraction  $V_f$ , subject to an applied transverse strain  $\varepsilon_x$  of 1%.

For Mode I, the presence of a free surface, and inversely the absence of a fully bonded fiber along the vertical direction, implies the absence of the counteracting upward-oriented vertical component of the displacement field due to the mismatch in Poisson’s ratios. This in turn translates into the constancy of the value of  $\Delta\theta$  corresponding to contact zone’s onset, always equal to  $60^\circ$ . For  $V_f = 30\%$ , Mode I is reduced when the spacing between debonds (in terms of fully bonded fibers in our models) decreases, but the magnitude of change is significant only when the spacing is reduced from a debond every 5<sup>th</sup> fiber to one every 3<sup>rd</sup>. For comparison, the difference of peak  $G_I$  values for  $V_f = 30\%$  between  $5 \times 1 - free$  and  $3 \times 1 - free$  is  $\sim 0.2 \frac{J}{m^2}$  (around 30% of the lower value), while between  $201 \times 1 - free$  and  $5 \times 1 - free$  is  $\sim 0.05 \frac{J}{m^2}$  (around 7%

of the lower value). A similar observation can be made for  $V_f = 60\%$ , but for larger spacings: no difference can be seen between the case of a debond placed every 101<sup>th</sup> and every 201<sup>th</sup> fiber. These observations suggest the existence of characteristic distance dependent on the fiber volume fraction which governs the interaction between debonds: in low  $V_f$  composites ( $V_f = 30\%$ ) the convergence to a non-interactive solution is faster (less interaction between debonded fibers in neighboring RUCs).

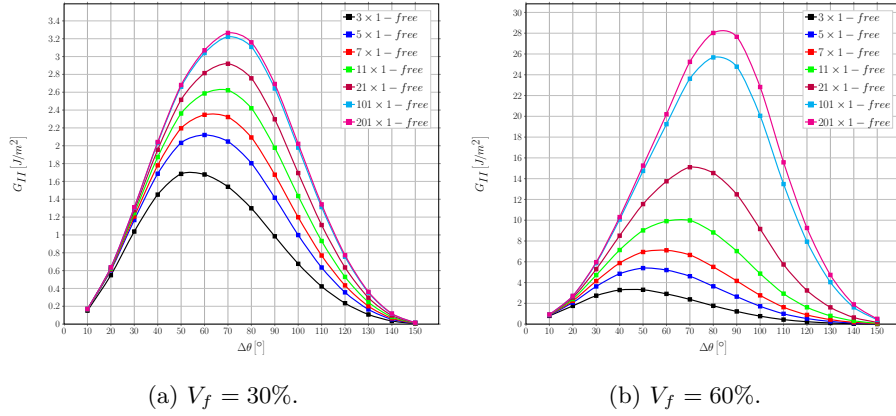


Figure 9: Effect of the interaction between debonds appearing at regular intervals on Mode II ERR in a single-ply laminate with a single layer of fibers at different levels of fiber volume fraction  $V_f$ , subject to an applied transverse strain  $\varepsilon_x$  of 1%.

Without constraint on the upper surface, the strain magnification effect creates a larger displacement gap in the  $x$ -direction, which increases Mode II for larger debonds. When debonds are far apart, the series of rigid elements in the ultra-thin composite row (constituted by fully bonded fibers and their surrounding matrix) creates higher  $x$ -strains in the element with the debonded fiber, which in turn generates higher tangential displacements at the crack tip for larger debonds. Conversely, when debonds are closer, the strain concentration in the debonded element is more similar to the applied strain (the magnification is reduced) and the tangential displacement component at the crack tip decreases for large  $\Delta\theta$ . This is the mechanism behind the change in the value of  $\Delta\theta$  for which the peak of  $G_{II}$  occurs: from 70° to 50° at 30%, and from

80° to 40° at 60% going from the higher to the smaller spacing of debonds.

265 Differently from Mode I, the presence of a characteristic distance is harder to establish. For  $V_f = 30\%$  (Fig. 9a), it seems reasonable to establish it at around 100 fully bonded fibers between each debond. For  $V_f = 60\%$  (Fig. 9b), the difference between models  $101 \times 1 - free$  and  $201 \times 1 - free$  is still sizable, thus preventing the establishment of such characteristic distance. It is possible to

270 observe, however, that the change between  $101 \times 1 - free$  and  $201 \times 1 - free$  is significantly smaller than between  $21 \times 1 - free$  and  $101 \times 1 - free$  ( $2 \left[ \frac{J}{m^2} \right]$  vs  $11 \left[ \frac{J}{m^2} \right]$ ), thus suggesting the existence of the characteristic distance outside the range studied. Nevertheless, one should question wheather the single row composite with free surface is an appropriate RUC for defining the upper bound

275 for  $G_{II}$ :  $G_{II}$  may be more affected by the free surface than by the effect of the interaction between debonds in the row.

### 3.3. Influence of rows of fully bonded fibers on debond's growth in RUCs with debonds in the central row

The effect of the presence of layers of fully bonded fibers on debond's growth

280 in a line of partially debonded fibers located at mid-thickness in UD composites is studied for Mode I (Fig. 10) and Mode II (Fig. 11) and fiber content equal to 30% (Figs. 10a and 11a) and 60% (Figs. 10b and 11b). The models treated are  $1 \times 3 - free$ ,  $1 \times 5 - free$ ,  $1 \times 7 - free$ ,  $1 \times 11 - free$ ,  $1 \times 21 - free$ ,  $1 \times 101 - free$  and  $1 \times 201 - free$ , corresponding to a UD composite with respectively 3, 5,

285 7, 11, 21, 101 and 201 rows of fibers (Fig. 2a) and each fiber debonded in the central row.

The results shown strengthen the considerations made in Sec. 3.1. It can in fact be seen in Fig. 10 that an increasing number of bonded fibers' rows across the thickness delays the onset of the contact zone to a debond of 70° in

290 size, due to the introduction of an additional positive component of the vertical displacement which translates into an opening displacement at the debond's tip. Comparing Fig. 9b with Fig. 11b, we observe that the presence of bonded fibers' rows significantly reduce the  $G_{II}$  and its maximum is shifted back to 60°, thus

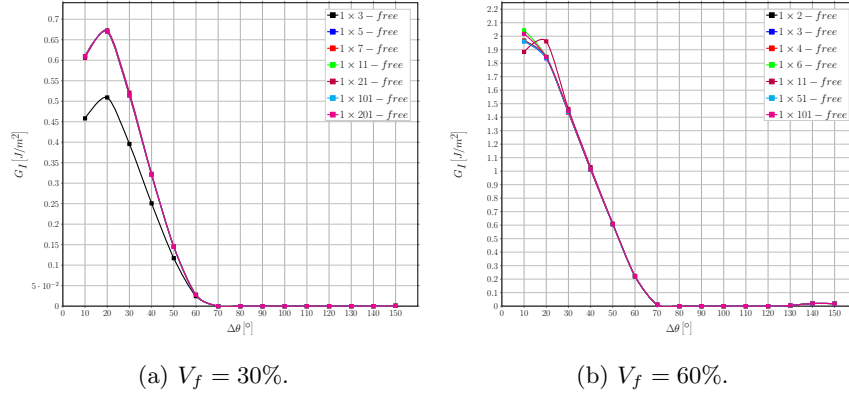


Figure 10: Influence of layers of fully bonded fibers on debond's growth in Mode I ERR in a centrally located line of debonded fibers at different levels of fiber volume fraction  $V_f$ , subject to an applied transverse strain  $\varepsilon_x$  of 1%.

confirming the hypothesis in Section 3.2 that the absence of  $G_{II}$  convergence with the increasing distance in a single-row composite is caused more by the free surface than by the interaction between debonds.

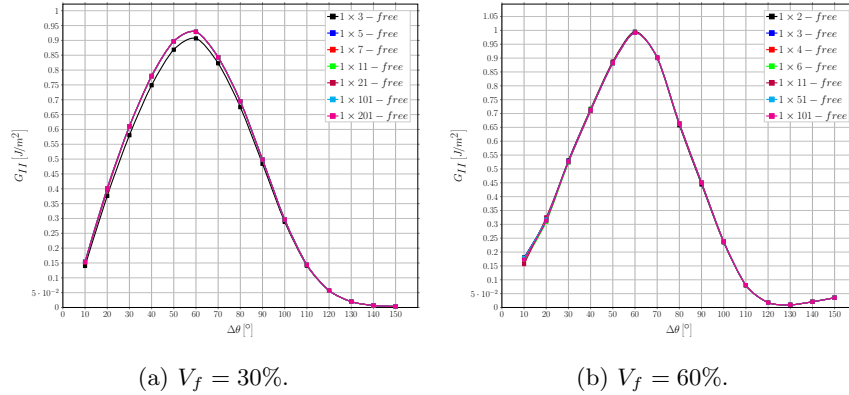


Figure 11: Influence of layers of fully bonded fibers on debond's growth in Mode II ERR in a centrally located line of debonded fibers at different levels of fiber volume fraction  $V_f$ , subject to an applied transverse strain  $\varepsilon_x$  of 1%.

The results of both Mode I and Mode II show that the introduction of an increasing number of fully bonded fibers's rows doesn't change the ERR calculated at the crack tip (the convergence is very fast). Some effect of the  $V_f$



300 (mostly on Mode I) can be observed at low fiber content (Figs. 10a and 11a), while for high fiber content the smaller model with only one fiber row above the partially debonded one is already representative.

### 3.4. Interaction between debonds in UD composites with multiple rows of fibers

The interaction of debonds appearing at regular intervals in UD compos-  
 305 ites with multiple rows of fibers is investigated using different combinations of horizontal debonds' spacing and number of rows of fibers across the thickness, corresponding to the models:  $3 \times 3 - free$ ,  $5 \times 3 - free$ ,  $5 \times 5 - free$ ,  $7 \times 3 - free$ ,  $7 \times 5 - free$ ,  $7 \times 7 - free$ ,  $11 \times 3 - free$ ,  $11 \times 5 - free$ ,  $11 \times 7 - free$ ,  $11 \times 11 - free$ ,  $21 \times 3 - free$ ,  $21 \times 5 - free$ ,  $21 \times 7 - free$ ,  $21 \times 11 - free$ ,  $21 \times 21 - free$ ,  
 310  $101 \times 3 - free$ ,  $101 \times 5 - free$ ,  $101 \times 7 - free$ ,  $101 \times 11 - free$ ,  $201 \times 3 - free$ ,  $201 \times 5 - free$ ,  $201 \times 7 - free$ ,  $201 \times 11 - free$  (Fig. 2b).

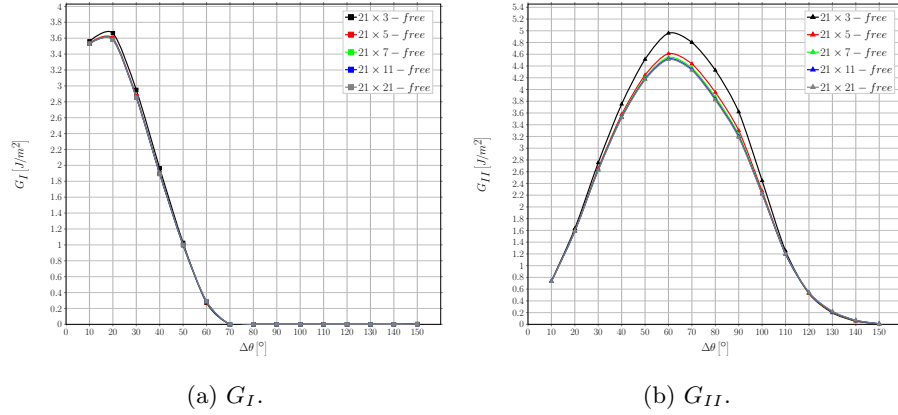


Figure 12: Effect on Mode I and Mode II ERR of the presence of an increasing number of rows of fully bonded fibers in UD composites with debonds appearing every  $10^{th}$  fiber (model  $21 \times k - free$ ).  $V_f = 60\%$  and  $\varepsilon_x = 1\%$ .

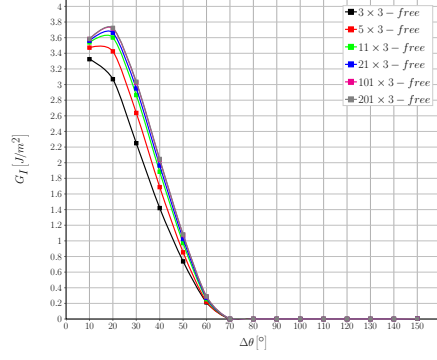
The results shown in Fig. 12 confirm the observations discussed in Sec. 3.2: the presence of fully bonded fibers across the thickness has a restraining effect on the ERR, that counteracts the magnification due to an increasing number of fully  
 315 bonded fibers in the horizontal direction. The interplay is further modulated by the fiber content. For Mode I, at high fiber content the contact zone onset

starts at  $70^\circ$  for  $V_f = 60\%$ , delayed with respect to the low fiber content case of  $60^\circ$ . Comparing Fig. 12 with Fig. 10b and Fig. 11b, it is furthermore possible to observe that the number of fully bonded fibers' rows necessary to reach convergence to a non-interacting solution in the vertical direction depends on the spacing of debonds in the central row. In Figures 10b and 11b the results for the  $1 \times 3 - free$  model (1 row below and above) are already representative of all the other cases; in Fig. 12 the solution doesn't change anymore once at least 3 rows below and above the central one are present, when convergence in both  $G_I$  and  $G_{II}$  is required.

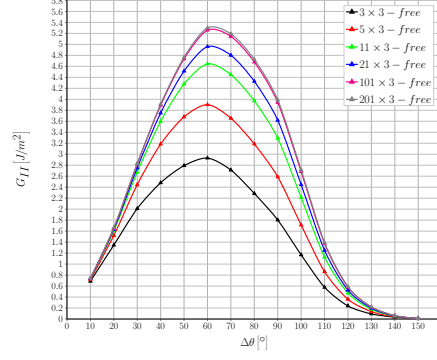
The results in Fig. 13 show that the converse is as well as true: the characteristic distance (in terms of fully bonded fibers) between debonds for which a non-interactive solution is attained changes in relation to the thickness of the UD composite (defined by the number of rows in the vertical direction). Mode I appears to be far less sensitive than  $G_{II}$  to the spacing of debonds in the horizontal direction when rows of fully bonded fibers are present above and below: in Fig. 13a the increase in the peak value of  $G_I$  is  $\sim 8\%$  going from model  $5 \times 3 - free$  to  $201 \times 3 - free$ , while  $< 5\%$  for larger spacings. In UDs of increased thickness, Figures 13c and 13e, the variation is further reduced. For Mode II, convergence to a non-interactive solution is reached with a spacing of 100 fully bonded fibers for a UD with 3 rows of fibers across the thickness ( $\frac{G_{II}^{201 \times 3}(60^\circ) - G_{II}^{101 \times 3}(60^\circ)}{G_{II}^{101 \times 3}(60^\circ)} \sim 0.7\%$ ), of 20 fibers in a UD with 5 rows ( $\frac{G_{II}^{101 \times 5}(60^\circ) - G_{II}^{21 \times 5}(60^\circ)}{G_{II}^{21 \times 5}(60^\circ)} \sim 4.3\%$ ) and of 10 fibers in a UD with 11 rows ( $\frac{G_{II}^{21 \times 11}(60^\circ) - G_{II}^{11 \times 11}(60^\circ)}{G_{II}^{11 \times 11}(60^\circ)} \sim 3.4\%$ ).

### 3.5. Comparison with the single fiber model with equivalent boundary conditions

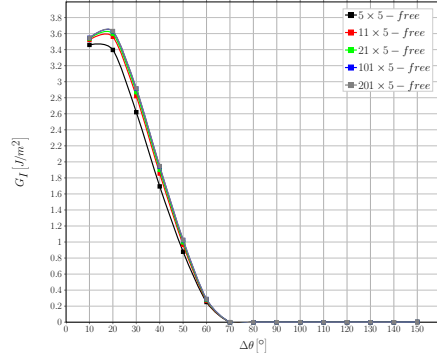
The comparison of the single fiber models with the corresponding multi-fiber models (Figs. 14, 15, 14 and 15) show that the former provide in general the lowest estimation of the ERR and correspond to the most damaged state of the laminate, i.e. the state in which the greatest number of debonds is present. The  $1 \times 1 - free$  or simply free model (Figs. 14 and 15), which represents a UD with a single layer of partially debonded fibers, agrees with the results of Sec. 3.2



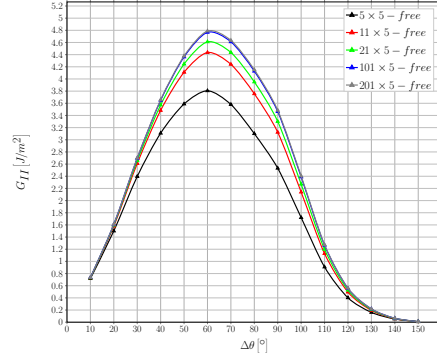
(a)  $k = 3$ ,  $G_I$ .



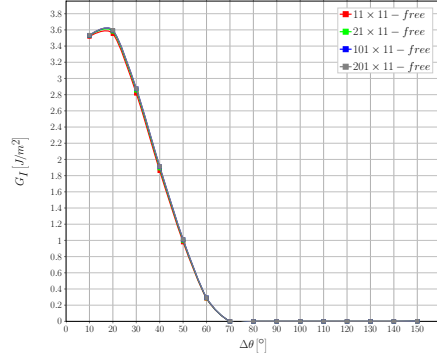
(b)  $k = 3$ ,  $G_{II}$ .



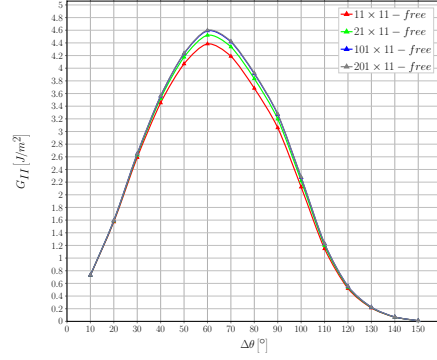
(c)  $k = 5$ ,  $G_I$ .



(d)  $k = 5$ ,  $G_{II}$ .



(e)  $k = 11$ ,  $G_I$ .



(f)  $k = 11$ ,  $G_{II}$ .

Figure 13: Effect on Mode I and Mode II ERR of increasing the spacing between debonds appearing in the central row of fibers in a UD composite with a fixed number of rows across the thickness.  $V_f = 60\%$  and  $\varepsilon_x = 1\%$ .

and constitutes the extreme case for UD with a single layer of fibers, i.e. the case in which all the fibers are partially debonded.

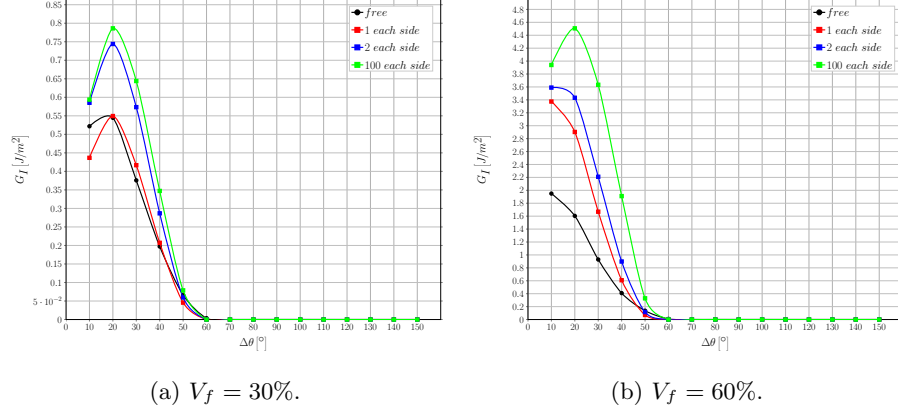


Figure 14: Comparison of Mode I ERR between the single fiber model with free upper boundary and the multiple fibers model with fibers only on the side at different levels of fiber volume fraction  $V_f$ , subject to an applied transverse strain  $\varepsilon_x$  of 1%.

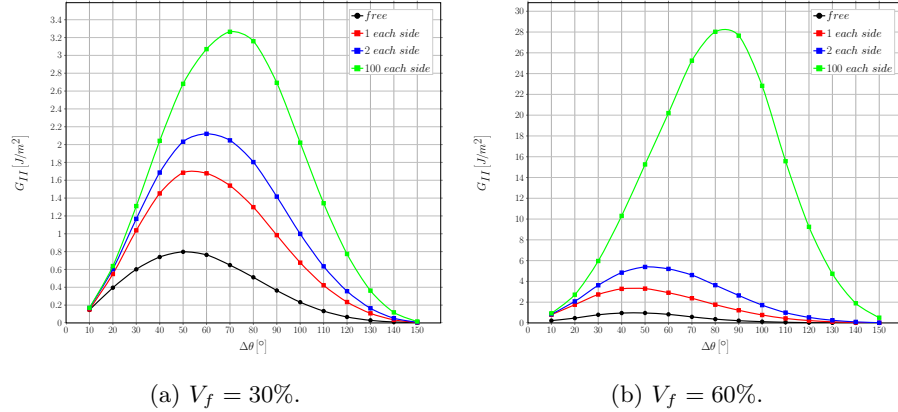


Figure 15: Comparison of Mode II ERR between the single fiber model with free upper boundary and the multiple fibers model with fibers only on the side at different levels of fiber volume fraction  $V_f$ .

The  $1 \times 1$  – *coupling* or coupling model (Figs. 16 and 17) underestimates consistently the ERR in Mode I and Mode II when compared with  $n \times k$  – *free* models, as it represents an infinitely thick UD with all the fibers partially

debonded. When compared with the  $1 \times k - free$  model, it shows interestingly a good agreement, especially in Mode I (Fig. 16a).

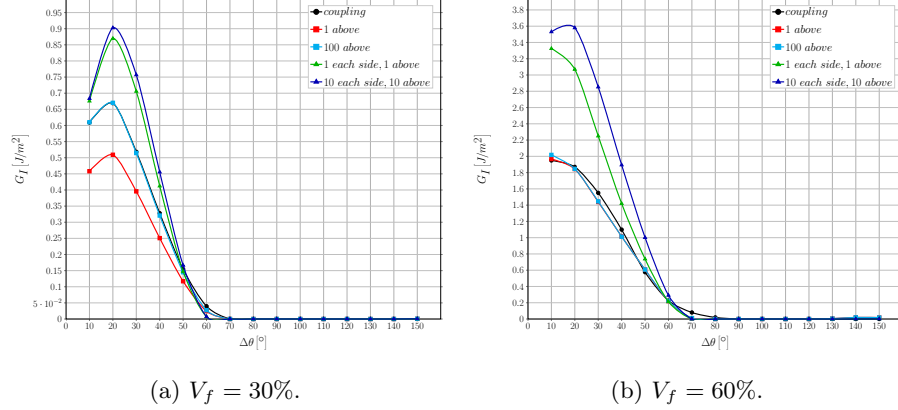


Figure 16: Comparison of Mode I ERR between the single fiber model with coupling conditions along the upper boundary and the multiple fibers model with fibers above and both above and on the side at different levels of fiber volume fraction  $V_f$ , subject to an applied transverse strain  $\varepsilon_x$  of 1%.

In Mode II, it shows a sizeable difference in the range  $50^\circ - 90^\circ$ , while its results coincide with those of the  $1 \times k - free$  model for other values of  $\Delta\theta$ . These observations point to the evidence that debonds' interaction has a significant effect in the loading direction and not in the transverse one. The lower estimates of  $G_{II}$  in the range  $50^\circ - 90^\circ$  are due to the presence of a debond of the same size in the fiber just above the central one (modeled by the coupling boundary condition), which leaves the strip of matrix between the two fibers free to deform away from both fibers due to Poisson's effect and thus favors Mode I and reduces Mode II. This translates in the lower estimates in Fig. 17 and to the delay in the appearance of the contact zone, particularly evident in Fig. 16b.

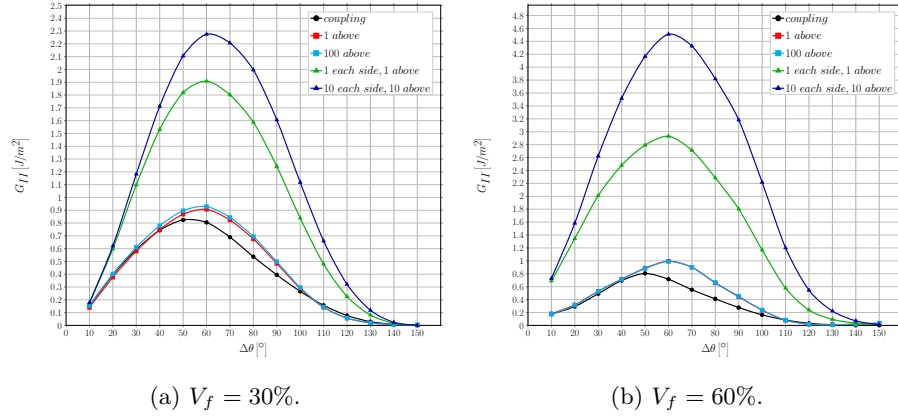


Figure 17: Comparison of Mode II ERR between the single fiber model with coupling conditions along the upper boundary and the multiple fibers model with fibers above and both above and on the side at different levels of fiber volume fraction  $V_f$ , subject to an applied transverse strain  $\varepsilon_x$  of 1%.

#### 4. Conclusions & Outlook

#### Acknowledgements

Luca Di Stasio gratefully acknowledges the support of the European School of Materials (EUSMAT) through the DocMASE Doctoral Programme and the European Commission through the Erasmus Mundus Programme.

#### References

- [1] Simulia, Providence, RI, USA, ABAQUS/Standard User's Manual, Version 6.12 (2012).
- [2] R. Krueger, Virtual crack closure technique: History, approach, and applications, Applied Mechanics Reviews 57 (2) (2004) 109. doi:10.1115/1.1595677.  
URL <https://doi.org/10.1115/1.1595677>
- [3] J. R. Rice, A path independent integral and the approximate analysis of strain concentration by notches and cracks, Journal of Applied Mechanics

35 (2) (1968) 379. doi:10.1115/1.3601206.

URL <https://doi.org/10.1115/1.3601206>

- 380 [4] C. Sandino, E. Correa, F. París, Numerical analysis of the influence of a nearby fibre on the interface crack growth in composites under transverse tensile load, *Engineering Fracture Mechanics* 168 (2016) 58–75. doi:10.1016/j.engfracmech.2016.01.022.

URL <https://doi.org/10.1016/j.engfracmech.2016.01.022>